iScience

CellPress
OPEN ACCESS

Article

Role of quiescent cells in the homeostatic maintenance of the adult submandibular salivary gland

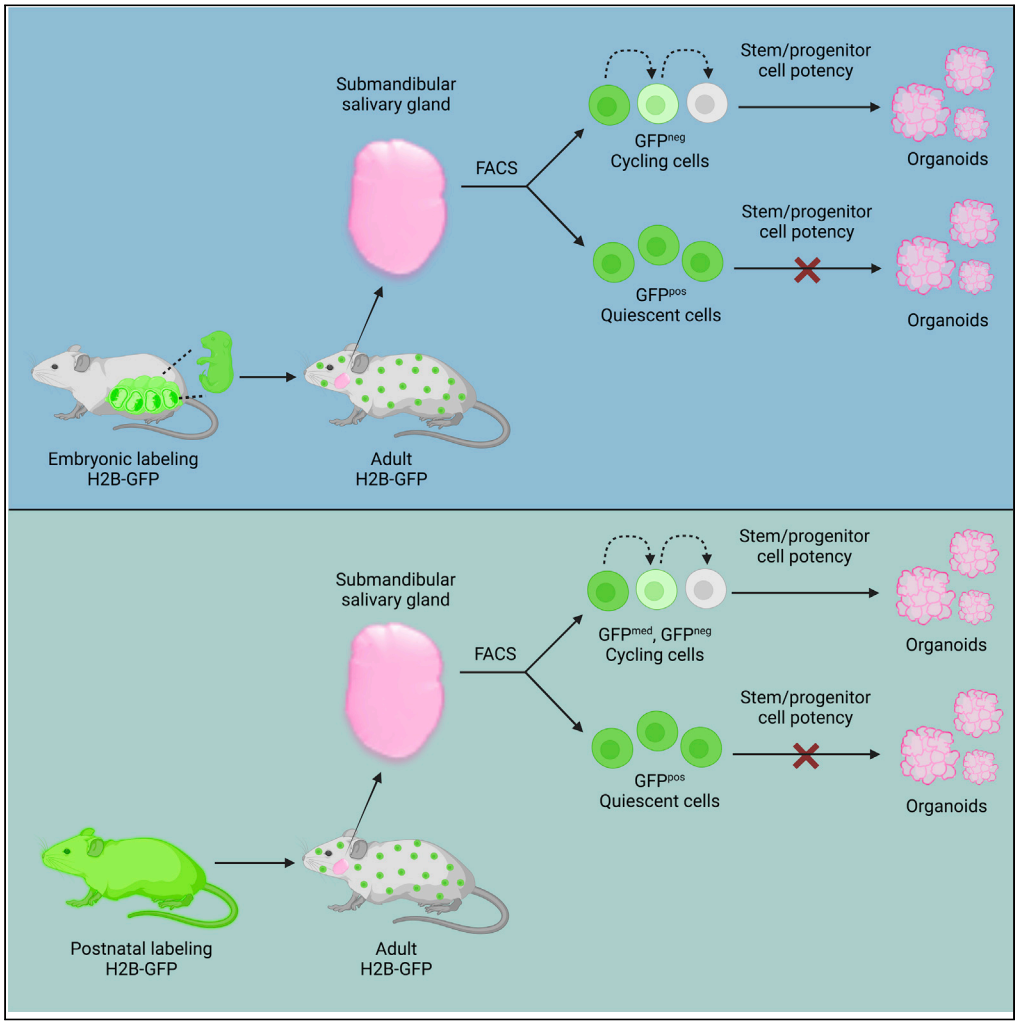

Paola Serrano Martinez, Martti Maimets, Reinier Bron, Ronald van Os, Gerald de Haan, Sarah Pringle, Robert P. Coppes

r.p.coppes@umcg.nl

Highlights

Embryonic quiescent cells do not retain stemness in the adult submandibular gland (SMG)

Postnatal quiescent cells do not exhibit stem/progenitor cell potency in the adult SMG

Quiescent cells do not contribute to the homeostatic maintenance of the murine SMG

Adult murine SMG stem/progenitor cells are likely to be an actively cycling population

Serrano Martinez et al., iScience 25, 105047 October 21, 2022
https://doi.org/10.1016/j.isci.2022.105047

iScience

CellPress
OPEN ACCESS

Article

Role of quiescent cells in the homeostatic maintenance of the adult submandibular salivary gland

Paola Serrano Martinez,[1,2,7,9] Martti Maimets,[1,2,6,9] Reinier Bron,[1,2,3] Ronald van Os,[4] Gerald de Haan,[4,8] Sarah Pringle,[5] and Robert P. Coppes[1,2,10,*]

SUMMARY

Stem/progenitor cells are required for maintenance of salivary gland (SG) function and serve as untapped reservoirs to create functional cells. Despite recent advancements in the identification of stem/progenitor pools, in the submandibular gland (SMG), a knowledge gap remains. Furthermore, the contribution to adult SMG homeostasis of stem/progenitor cells originating from embryonic development is unclear. Here, we employ an H2B-GFP embryonic and adult pulse-and-chase system to characterize potential SMG stem/progenitor cells (SGSCs) based on quiescence at different stages. Phenotypical profiling of quiescent cells in the SMG revealed that label-retaining cells (LRCs) of embryonic or adult origin co-localized with CK8+ ductal or vimentin + mesenchymal, but not with CK5+ or CK14 + stem/progenitor cells. These SMG LRCs failed to self-renew *in vitro* while non-label retaining cells displayed differentiation and long-term expansion potential as organoids. Collectively, our data suggest that an active cycling population of cells is responsible for SMG homeostasis with organoid forming potential.

INTRODUCTION

Adult stem cells are undifferentiated and long-lived cells, which have a remarkable capacity to replenish themselves through self-renewal and to give rise to either one (unipotent) or more (multipotent) downstream differentiated cell lineages. This original definition has evolved to consider stem cells as a heterogeneous cellular population with different transcriptional profiles, self-renewal ability, adaptability, and plasticity to maintain tissue homeostasis and regeneration (Chacón-Martínez et al., 2018). The application of adult stem cells as a treatment for radiation-induced damage, immune diseases, and aging (cell therapy) has garnered much interest. Given their importance for the long-term maintenance of tissues, stem cells are often thought to be quiescent, leaving most of the tissue regeneration to transiently dividing but committed progeny (Hsu and Fuchs, 2012). Many stem cells in the mammalian body are only called into action for initiation of repair following injury (Fuchs, 2009). Stem cell quiescence is critical to ensure lifelong tissue maintenance and to protect the stem cell pool from premature exhaustion, which may culminate in failure to repair tissue in response to injury (van Velthoven and Rando, 2019). Even though quiescence is a characteristic of many adult stem cells, it is not a universal feature. In some cases, such as the skin (Clayton et al., 2007) or intestine (Barker et al., 2007), stem cells undergo daily turnover as part of their normal homeostatic process. Interestingly, the cycling Lgr5+ stem cell population in the intestine coexists with the +4 cells, a reservoir of quiescent stem cells (Tetteh et al., 2016; Jadhav et al., 2017). In other tissues, such as skeletal muscle (Collins et al., 2005), blood (Wilson et al., 2008; Foudi et al., 2009), or liver (MacDONALD, 1961; Magami et al., 2002; Miyaoka et al., 2012; Pepe-Mooney et al., 2019), stem cells undergo extremely low or no division during normal homeostasis but can respond efficiently to stimuli or injury by entering the cell cycle.

In the case of the salivary gland (SG), a large body of work suggests and supports the presence of multiple stem/progenitor cell populations. Ligation of the major excretory duct, resulting in tissue degeneration, and subsequent de-ligation experiments have demonstrated the extensive regeneration capacity of the SG (Takahashi et al., 2004a, 2004b; Osailan et al., 2006; Cotroneo et al., 2008; Cotroneo et al., 2010). Multiple markers commonly identified in stem/progenitor cells of several tissues have been shown to be

[1]Department of Biomedical Sciences of Cells and Systems, Section Molecular Cell Biology, University Medical Center Groningen, University of Groningen, Antonius Deusinglaan 1, 9713 AV Groningen, the Netherlands

[2]Department of Radiation Oncology, University Medical Center Groningen, University of Groningen, PO Box 30001, 9700 RB Groningen, the Netherlands

[3]Department of Biomedical Engineering, University Medical Center Groningen, Antonius Deusinglaan 1, 9713 AV Groningen, the Netherlands

[4]Department of Biology of Aging, Section Stem Cell Biology, European Research Institute for the Biology of Aging (ERIBA), University Medical Center Groningen, University of Groningen, Antonius Deusinglaan 1, 9713 AV Groningen, the Netherlands

[5]Department of Rheumatology and Clinical Immunology, University Medical Center Groningen, University of Groningen, 9700 RB Groningen, the Netherlands

[6]Present address: Biotech Research & Innovation Centre, University of Copenhagen, Ole Maaløes Vej 5, DK-2200 Copenhagen N, Denmark

[7]Present address: Ocular Angiogenesis Group, Department of Ophthalmology, Amsterdam UMC, Meibergdreef 15, 1105 AZ Amsterdam, the Netherlands

[8]Present address: Department of Hematopoiesis, Sanquin Research, and Landsteiner Laboratory, Academic

Continued

present in the submandibular gland (SMG), such as c-Kit (Hisatomi et al., 2004; Lombaert et al., 2008, 2013; Nanduri et al., 2011), stem cell antigen 1 (Hisatomi et al., 2004; Lombaert et al., 2008), cytokeratin 5 (CK5) (Knox et al., 2010; Lombaert et al., 2013), cytokeratin 14 (CK14) (Lombaert et al., 2013), CD133 (Nanduri et al., 2011), $CD24^{high}/CD29^{high}$ (Nanduri et al., 2011), Lin−CD24+/c-Kit+/Sca1+ (Xiao et al., 2014), $EpCAM^{high}$ (Maimets et al., 2016), and SOX2 (Emmerson et al., 2018). Interestingly, cells isolated directly from SMGs of adult mice and grown as organoids under defined conditions can be expanded into clinically relevant numbers of SGSCs *in vitro* (Nanduri, 2014; Maimets et al., 2016). In transplantation experiments, these SGSCs are able to engraft into the donor tissue, salvaging irradiation-damaged epithelium (Lombaert et al., 2008; Nanduri, 2014; Maimets et al., 2016; Pringle et al., 2016). Lineage tracing experiments have demonstrated that during homeostasis, the duct and acinar cell populations may be separately sustained (Aure et al., 2015). Conversely, under conditions of severe SG damage, acinar cell regeneration appears to be performed by both ductal and acinar cells (Aure et al., 2015; Weng et al., 2018). Most of these studies investigated the localization and phenotype of SGSC during regeneration; however, the SGSC importance for homeostasis remains ambiguous.

Previously, using label retention as a surrogate marker for quiescence, label-retaining cells (LRCs) have been found distributed throughout the parenchyma of the murine SG (Kim et al., 2008; Kimoto et al., 2008; Chibly et al., 2014; Kwak and Ghazizadeh, 2015). However, the identity of SMG LRCs as an active or quiescent stem/progenitor population has been controversial. In one study, cells labeled with EdU during early postnatal development and followed during adulthood displayed proliferation and differentiation potential, while expressing markers of putative salivary progenitors CK5, CK14, and c-kit (Chibly et al., 2014). EdU, however, needs at least one cell division to label cells. Therefore in a second study, cells marked by the cell cycle state independent histone H2B-GFP during embryonic and early postnatal development, and followed into adulthood, could be mapped to the more differentiated ductal compartments (Kwak and Ghazizadeh, 2015). Moreover, these cells did not display the characteristics of quiescent stem/progenitor cells, including expression of stem/progenitor cell markers, mobilization in response to injury, and clonogenicity in culture. These data suggest that the postnatal SMG is sustained by an active cycling stem/progenitor population (Kwak and Ghazizadeh, 2015). Unfortunately, the assays used in both of the studies did not permit an optimal measurement of self-renewal and differentiation of LRCs.

Here, we utilized the H2B-GFP system (Foudi et al., 2009) and derived organoids to study the contribution of quiescent stem/progenitor cells in the homeostatic maintenance of the SMG. We labeled quiescent cells at different times in SMG development ("pulse") which enabled the study of the SMG dynamics from embryonic and adult phases. Manipulating the subsequent "chase" periods allowed us to interrogate the nature of LRC localization within the SMG. Furthermore, challenging different LRC populations in *in vitro* SMG organoid formation assays (Maimets et al., 2016) as a surrogate measure of stem/progenitor cell potential permitted us to directly estimate the regenerative potential of these cells.

RESULTS

Embryonic pulse-adult chase experiments reveal slow-cycling cells in excretory and striated ducts of the adult SMG

We assessed the feasibility of using label retention to select for slow-cycling SGSCs, given that a slower division rate is a characteristic of many adult stem cells (Post and Clevers, 2019). In order to visualize and trace the fate of infrequently dividing LRCs in the adult SMG, we used a mouse strain that allows ubiquitous, doxycycline-inducible expression of an H2B-GFP fusion protein (Foudi et al., 2009). To investigate the contribution of embryonic precursors to the adult SGSC pool, the H2B-GFP label was induced in pregnant female mice at embryonic day 18 (E18) by doxycycline administration, until birth (Figure 1A, Pulse). After this time point, the loss of fluorescence in the SMG was monitored (Figure 1A, Chase). The SMG is a complex organ with a three-dimensional (3D) ductal organization. To explore the presence of the H2B-GFP label in the SMG immediately after the pulse, we developed a 3D confocal imaging strategy allowing *in situ* visualizations of expansive areas of the SMG tissue architecture (Figure 1B and Video S1). Ductal (Figure 1B, arrows) and acinar (Figure 1B, arrowheads) compartments could be observed at high cellular resolution scanning up to 2.5 mm of tissue. In agreement with the 3D images, immunostaining using anti-GFP antibody on paraffin SMG sections confirmed labeling of ductal (Figure 1C, arrows) and acinar (Figure 1C, arrowheads) as well as myoepithelial (Figure 1C, asterisk) cells, readily distinguished by their respective shape and position within the gland. Next, we examined the cells retaining the H2B-GFP label over time within the SMG. For optimal imaging, we used a clearing technique (Yang et al., 2014) (Figures 1D

Medical Center, University of Amsterdam, the Netherlands

[9]These authors contributed equally

[10]Lead contact

*Correspondence: r.p.coppes@umcg.nl

https://doi.org/10.1016/j.isci.2022.105047

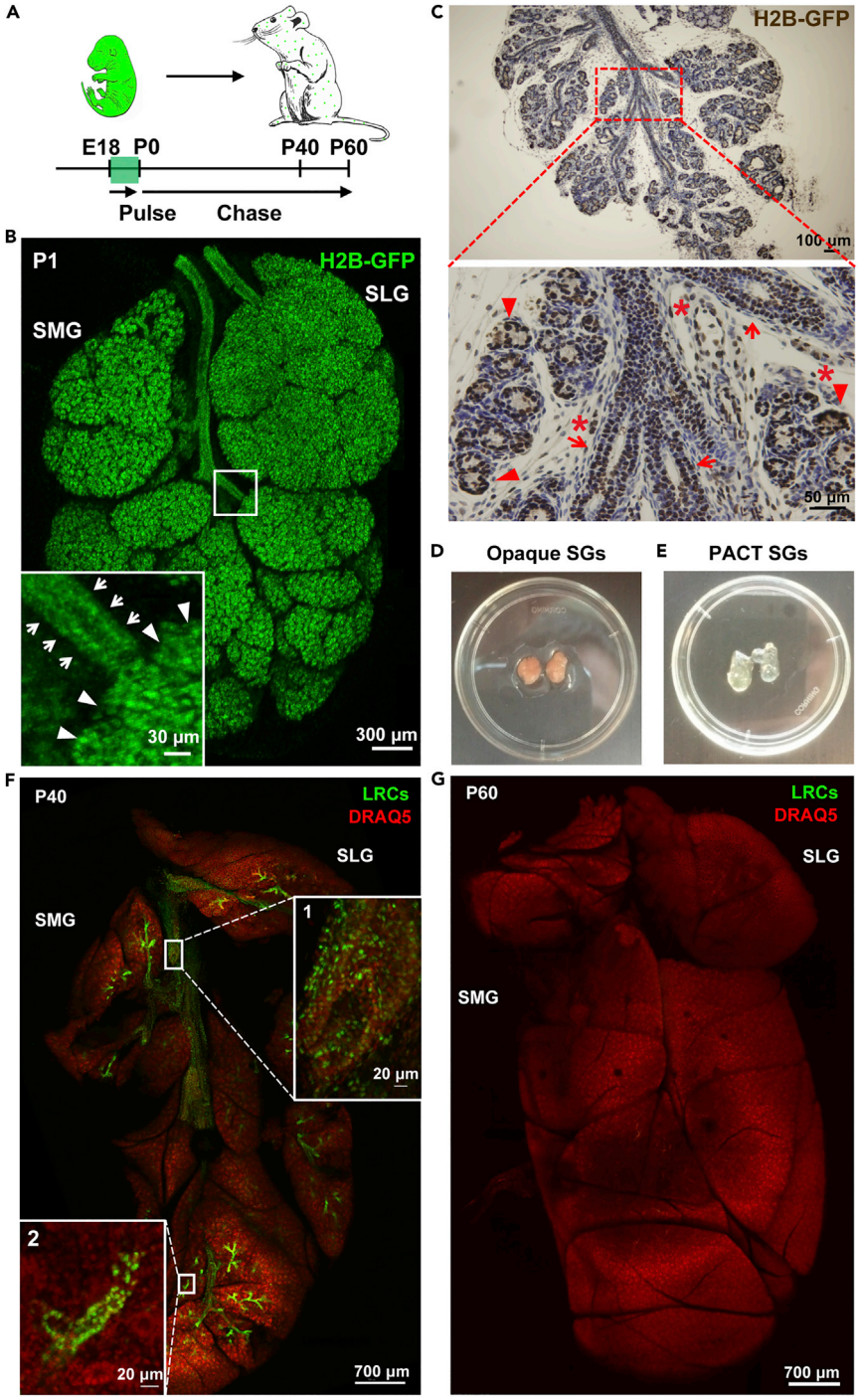

Figure 1. Schematic model for the chase of embryonic slow-cycling cells in the SMG and the monitoring of their fate

(A) Experimental strategy.

(B) 3D confocal reconstruction of a whole-mounted 1-day-old (P1) SG. Expression of the H2B-GFP fusion protein is detected in ductal (arrows) and acinar compartments (arrowheads) of the SMG. Scale bars 300 µm (whole-mount) and 30 µm (enlargement). SLG, sublingual gland.

(C) Immunohistochemical GFP staining in paraffin SMG sections shows the expression of the H2B-GFP fusion protein in ductal (arrows), acinar (arrowheads), and myoepithelial (asterisk) cells. Scale bars 100 µm (upper panel) and 50 µm (lower panel).

Figure 1. *Continued*
(D) 4% formaldehyde fixed SGs with milk appearance.
(E) PACT-processed SGs with transparent appearance.
(F) Whole-mount 3D confocal images of 40-day old (P40) SG showing the position of LRCs in the excretory duct (Panel 1) and in striated ducts (Panel 2) of the SMG. Scale bars 700 μm (whole-mount) and 20 μm (Panel 1, 2). Nuclei counterstained with DRAQ5.
(G) Whole-mount of a 60-day-old (P60) SG showing no visible GFP^+ cells. Scale bar 700 μm. Nuclei counterstained with DRAQ5.

and 1E) showing at 40 days of chase a dramatically reduced number of GFP-expressing cells. Notably, LRCs carrying H2B-GFP label were observed chiefly in ductal (Figure 1F and Video S2) and not in acinar compartments as distinguished by their respective shape and position in the gland. Specifically, we encountered GFP^+ cells in excretory ducts (Figure 1F, panel 1) and striated ducts (Figure 1F, panel 2). These data suggest that embryonic precursors with slow turnover reside in excretory and striated ducts of the SMG in the adult mouse, locations that were previously suggested to contain stem/progenitor cells (Lombaert et al., 2008; Maimets et al., 2016).

Marker expression profile of LRCs from embryonic development is not reminiscent of SGSCs

To determine the fate of embryonic LRCs acquired after SMG maturation, we analyzed the remaining H2B-GFP labeling following a 60-day chase period. At this time point, we were not able to detect LRCs by large-scale microscopy possibly due to the small number of remaining LRCs (Figure 1G). Therefore, we performed co-expression analysis of H2B-GFP with CK14 and CK5, markers associated with SG stem/progenitor cells (Knox et al., 2010, 2013; Lombaert et al., 2013), on SMG tissue sections (Figures 2). We observed LRCs scattered throughout the parenchyma of the SMG most prominently in ductal compartments (Figure 2). The expression of CK14 was found in the basal layer of excretory ducts (Figures 2A and 2B) but was not co-localized with ductal LRCs (Figure 2B, arrows). Similarly, CK5-expressing cells were confined to basal cells in the excretory ducts (Figures 2C and 2D) but did not overlap with LRCs (Figure 2D, arrows). Conversely, the ductal marker cytokeratin 8 (CK8) (Figures 2E and 2F) expressing cells did co-localize with LRCs in the luminal part of the excretory ducts (Figure 2F, arrows). Acinar cells are easily recognizable based on their morphology. We were not able to observe LRCs in the acinar cell compartment. To characterize the remainder of LRCs residing outside of the epithelial compartment and the role of these cells in glandular development, we co-immunostained SMG sections for the mesenchymal marker vimentin (Eriksson et al., 2009) (Figures 2G and 2H). GFP co-expression of vimentin was observed in few cells (Figure 2H, arrows) which seems suggestive of a small compartment of slow-dividing mesenchymal cells. However, the role of these cells in tissue homeostasis warrants further research. Overall, these data suggest that embryonic precursors are not putative SGSCs.

Embryonic LRCs do not promote the growth of SMG organoids *in vitro*

We next sought to assess the potential of embryonic LRCs remaining after a 60-day chase period to form SMG organoids (Figure 3A). Organoid forming potential can be employed as a surrogate to measure the self-renewal ability of a stem/progenitor cell population (Maimets et al., 2016). SMGs were isolated and digested into single-cell suspension and depleted of $CD45^+$ and $TER119^+$ hematopoietic and $CD31^+$ endothelial cells (Lin^-) (Figure 3B, left panel). Next, SMG cells were subdivided into three cell populations, GFP^{high}, GFP^{med}, and GFP^{neg} (Figure 3B, right panel) using fluorescence-activated cell sorting (FACS). The resultant proportions of cells in the GFP^{high} population were 1.8 $\pm$ 0.2%, in GFP^{med} 13.4 $\pm$ 1.1%, and in GFP^{neg} 84.9 $\pm$ 1.1% (Figure 3C). Purified cells were embedded in Matrigel and supplemented with WRY medium (Maimets et al., 2016). GFP^{high} (Figures 3D and 3G) and GFP^{med} (Figures 3E and 3G) populations were unable to efficiently initiate cultures (<0.06%) while GFP^{neg} cells successfully generated organoids (Figures 3F and 3G) (0.47 $\pm$ 0.1% organoid forming efficiency). Next, organoids derived from single GFP^{neg} cells were dissociated and seeded into Matrigel supplemented with WRY medium. Within the period of three passages (3 weeks), these cultures displayed exponential growth (Figure 3H) similar to what was observed previously in wild-type organoids (Nanduri, 2014; Maimets et al., 2016). In addition, as cells derived from the GFP^{neg} population were passaged, and an increase in the ability to form organoids was observed (Figure 3I). Taking this together, the self-renewal potential of embryonic slow-cycling cells indicates that these LRCs do not include cells with *in vitro* proliferation potential and therefore may not represent stem/progenitor cells in the SMG.

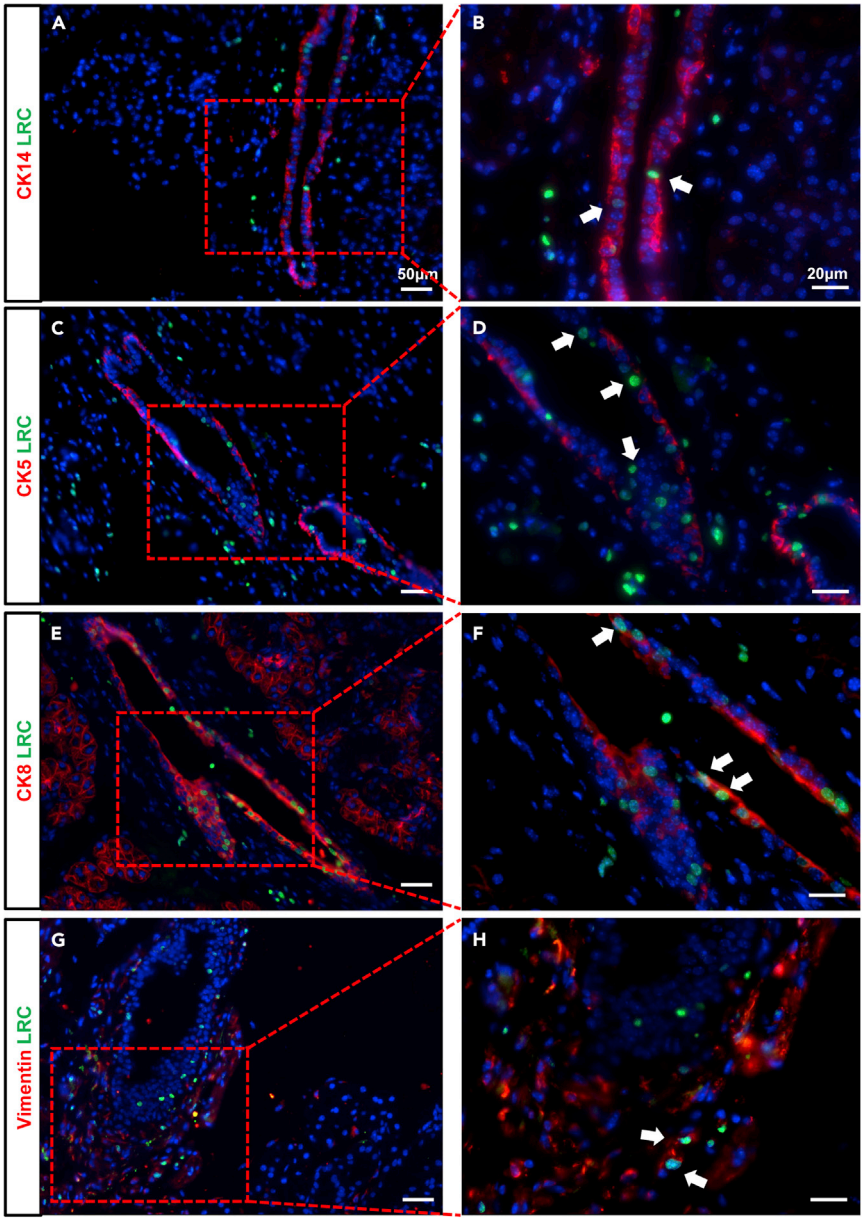

Figure 2. Few embryonic LRCs co-localize with CK8$^+$ ductal luminal or Vimentin$^+$ mesenchymal cells in the SMG

(A–D) Double immunofluorescence for (A–B) GFP and CK14 and (C–D) GFP and CK5 show no overlap between LRCs (arrows) and CK14$^+$ and CK5$^+$ cells in the SMG ductal compartment.

(E–H) Double immunofluorescence for (E–F) GFP and CK8 and (G–H) GFP and Vimentin reveal co-localization (arrows) of LRCs and ductal luminal cells (CK8$^+$), and LRCs and mesenchymal cells (Vimentin$^+$) in the SMG. Paraffin SMG sections, nuclei counterstained with DAPI. Scale bars 50 μm (left panel) and 20 μm (right panel).

Adult LRCs do not acquire a SMG stem/progenitor cell fate

Our previous results suggest the lack of a SMG quiescent stem/progenitor cell population with an embryonic origin. We next asked whether such cells are developed after weening because of the physiological change in the SG composition. To investigate the quiescent cell population in adulthood, we used a pulse-chase strategy in adult H2B-GFP mice. Initially, doxycycline was administered to 60-days-old animals for 5 days, followed by the assessment of the GFP label in the SMG (Figure S1A). After a pulse of 5 days, up to 22.8 ± 0.6% of the SMG cells were labeled as determined by FACS analysis (Figures S1B and S1C), including all the cell types within the SMG (myoepithelial cells, acinar cells, striated duct cells, intercalated

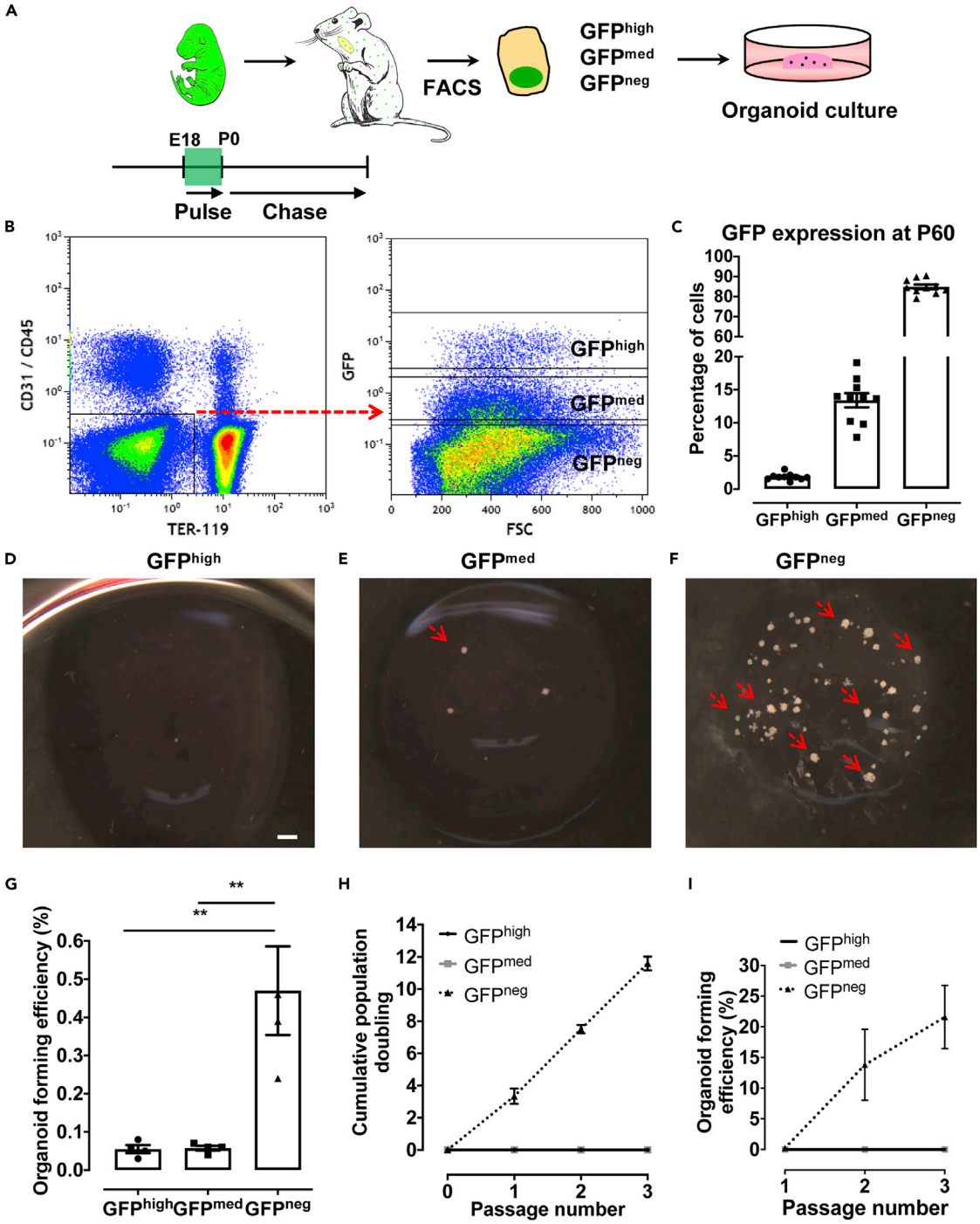

Figure 3. Regenerative potential of embryonic SMG LRCs

(A) Experimental strategy.

(B) Representative FACS gating strategy for the analysis of LRCs in the SMG. The left panel shows the exclusion of lineage marker-expressing cells. The right panel depicts the distribution of GFP^{high}, GFP^{med}, and GFP^{neg} cells in dissociated adult mouse SMG. FSC, forward scatter.

(C) Fractions of GFP^{high}, GFP^{med}, and GFP^{neg} cells in P60 adult murine SMG. Data are represented as mean ± SEM.

(D–F) DIC images showing the outgrowth (arrows) of SMG (D) GFP^{high}, (E) GFP^{med}, and (F) GFP^{neg} cell populations after 12 days in culture.

(G) Organoid formation efficiency of sorted SMG GFP^{high}, GFP^{med}, and GFP^{neg} cells. Data are represented as mean ± SEM (**$p < 0.01$).

(H) Population dynamics plot of SMG GFP^{high}, GFP^{med}, and GFP^{neg} cells. Data are represented as mean ± SEM.

(I) Organoid formation kinetics of SMG GFP^{high}, GFP^{med}, and GFP^{neg} cells during serial passaging. Data are represented as mean ± SEM.

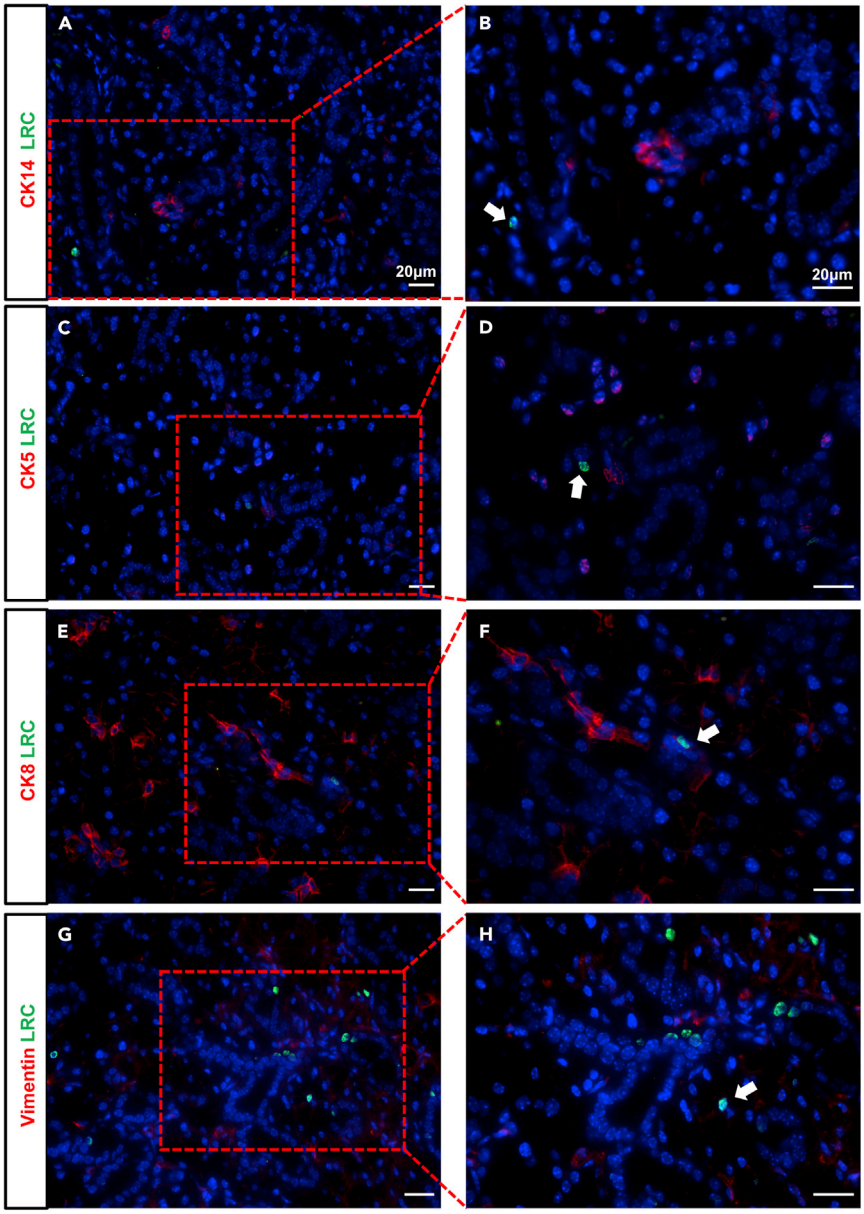

Figure 4. Few adult SMG LRCs co-express CK8 or vimentin markers

(A and B) Immunofluorescence for GFP/CK14 and (C and D) GFP/CK5 showing no overlapping between quiescence (arrows) and $CK14^+$ and $CK5^+$ cells in the SMG.

(E and F) Immunofluorescence staining for GFP/CK8 and (G and H) GFP/Vimentin showing co-localization (arrows) of LRCs with ductal ($CK8^+$) and mesenchymal the marker Vimentin ($Vimentin^+$) in the SMG. Paraffin SMG sections, nuclei counterstained with DAPI. Scale bars 20 μm.

duct cells, and excretory duct cells) as shown by immunohistochemistry (IHC) staining (Figure S1D). Next, the pulse of 5 days was followed by a chase period of 125 days (Figure S2A), covering at least 2 SG cellular turnover cycles (Zajicek et al., 1989). To characterize the cellular fate to which adult LRCs commit after full SMG development, we analyzed the co-expression of H2B-GFP with the previously described SG markers. Quiescent GFP-expressing cells were scarcely observed through the SMG tissue (Figures 4A–4H). The expression of GFP + LRCs did not colocalize with the ductal progenitor markers CK14 and CK5 (Figures 4A–4D, arrows). Interestingly, we noted co-expression of the CK8 ductal marker (Figures 4E and 4F, arrows) and mesenchymal marker Vimentin (Figures 4G and 4H, arrows) by a GFP + LRC, suggesting a potential to differentiate into ductal and stromal cells. Lastly, based on the acinar cellular morphology,

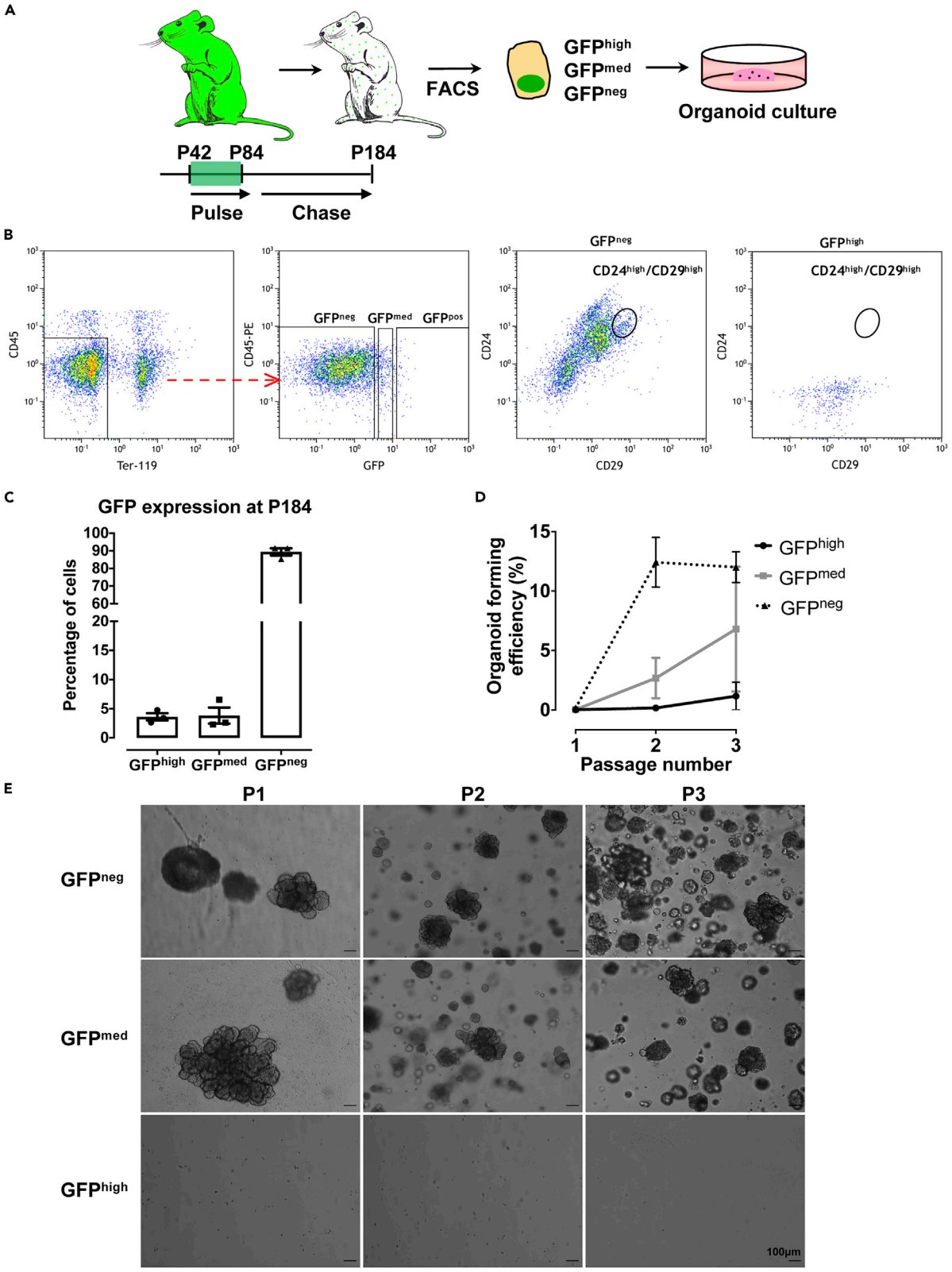
A
FACS
GFPhigh
GFPmed
GFPneg
Organoid culture
P42
P84
P184
Pulse
Chase
B
CD45
Ter-119
CD45-PE
GFP
GFPneg
GFPmed
GFPpos
CD24
CD29
CD24high/CD29high
C
GFP expression at P184
Percentage of cells
D
Organoid forming efficiency (%)
Passage number
E
P1
P2
P3
100μm

Figure 5. Dividing cells in the adult SMG exhibit stem/progenitor cell potential

(A) Pulse-chase strategy.

(B) Flow cytometry analysis of the isolated SMG GFP^{neg}, GFP^{high} populations for $CD24^{high}/CD29^{high}$ expression. The data showed the presence of $CD24^{high}/CD29^{high}$ expression in the GFP^{neg} population.

(C) Quantification of the proportion of sorted SMG GFP^{neg}, GFP^{med}, and GFP^{high} cells after 100 days of chase. Data are represented as mean ± SEM.

(D) Self-renewal potential of SMG GFP^{neg}, GFP^{med}, and GFP^{high} cells. Data are represented as mean ± SEM.

(E) Representative images of organoid growth of the three groups of SMG isolated cells. Scale bars 100 μm.

we did not observe LRCs in the acinar SMG compartment. These results are reminiscent of our previous observations regarding the cell fate that embryonic LRC acquire postnatally. Our data would suggest that adult LRCs do not acquire a stem/progenitor cell phenotype, but some quiescent LRC cells may mature into CK8+ and vimentin + cells in the SMG.

Adult SMG LRCs do not display higher *in vitro* proliferative potential

As a next step to understanding quiescence in the SMG, we sought to probe the regenerative potential of the quiescent and non-quiescent stem/progenitor cells. SMGs of the pulsed-chased mice were excised, and single-cell isolation was performed, showing 1.7 ± 0.3% GFP^{pos} and 98.2 ± 0.3% GFP^{neg} Lin- FACS-sorted single cells (Figures S2A and S2B). Resultant single cells were embedded in Matrigel and subjected to organoid culture conditions. The assessment of the organoid forming potential of GFP^{neg} and GFP^{pos} cells depicted that both populations were able to initiate organoid formation (Figure S2C), 0.3 ± 0.1% and 0.2 ± 0.1%, respectively (Figure S2D). Next, the organoids were passaged as described above. After 3 weeks (3 passages), both GFP^{pos} and GFP^{neg} populations exhibited a similar self-renewal potential with exponential growth shown by the organoid forming efficiency and the cumulative population doublings (Figures S2E and S2F). These data suggest that adult LRCs in the SMG do not display a higher *in vitro* stem/progenitor cell potential compared to their non-labeled counterparts.

Cycling cells constitute the populations with stem/progenitor cell potential in the adult SMG

It remains possible that due to the limited efficiency of the 5 days pulse strategy, the label of some quiescent cells that might have an important contribution in the adult SMG maintenance may have been missed. In order to circumvent this technical limitation, we extended the doxycycline pulse to 42 days, administered to 42-days-old (P42) H2B-GFP mice (Figure S3A). This strategy allowed to increase the labeling efficiency to 53.3 ± 3.8% of the SMG cells (Figures S3B and S3C), marking all the cell types within the SMG (myoepithelial cells, acinar cells, striated duct cells, intercalated duct cells, and excretory duct cells) (Figure S3D). Next, to analyze the regenerative potential of none cycling LRCs (GFP^{high}) and cells that have undergone some proliferation (GFP^{med}) or more (GFP^{neg}), the pulse of 42 days with doxycycline was followed by a chase period of 100 days (Figure 5A) and Lin^{-} GFP^{neg}, GFP^{med}, and GFP^{high} SMG populations were sorted using FACS (Figures 5A and 5B). The resulting isolated populations correspond to 89.4 ± 2.0% GFP^{neg} cells, 3.8 ± 1.4% GFP^{med} cells, and 3.6 ± 0.6% GFP^{high} cells (Figure 5C). $CD24^{high}/CD29^{high}$ FACS expression analysis revealed that the GFP^{neg} cells expressed these markers (Figure 5B, right two panels). Furthermore, the GFP^{neg} and GFP^{med} cells were able to self-renew over passaging, while the GFP^{high} population alone lacked this ability (Figures 5D and 5E). Interestingly, even when extending the labeling period and increasing the percentage of labeled cells within the SMG, we obtained similar results. This indicates that we were not able to find rare LRCs that could exhibit stemness potential. Overall, these findings suggest that adult quiescent stem/progenitor cells of postnatal origin do not exhibit stemness potential, whereas dividing cells constitute a SGSC population in the SMG.

DISCUSSION

Accurate identification of SGSCs remains one of the major hurdles to overcome in understanding SG tissue maintenance and regeneration. A property of some tissue stem cells is their quiescence in terms of the cell cycle. Dormancy of stem cells is believed to provide selective survival advantage under unfavorable conditions and to protect them from stress (Cheung and Rando, 2013). In this study, we employed a cell-state independent H2B-GFP pulse-chase system to determine the dynamics of stem/progenitor cells in the mouse SMG and to characterize the putative quiescent stem/progenitor cell population that may exist within. We provide evidence that quiescent cells within the SMG, of both embryonic and adult origin, do not display characteristics of tissue-specific stem/progenitor cells. Despite H2B-GFP labeling of the SMG parenchyma following the embryonic pulse period, we found no proof of stem/progenitor cell potency of quiescent cells derived from the embryonic development, in the context of the adult SMG. Considering that the SMG continues to develop postnatally and

stem/progenitor cells could potentially be activated after birth (Kwak et al., 2016), we additionally employed a pulse-chase strategy in postnatal H2B-GFP mice. Adult LRCs of postnatal origin also did not constitute a population with stem/progenitor characteristics, similar to LRCs from embryonic origin.

Studies previously conducted to discern quiescent stem cells in the SG have resulted in contrasting observations. In one study (Chibly et al., 2014), LRCs marked by EdU identified a cell population expressing SG putative progenitor markers with *in vitro* proliferative potential. In a second study, LRCs targeted with a histone H2B-GFP model were mapped to the more differentiated ductal compartments and lacked proliferative potential *in vitro* (Kwak and Ghazizadeh, 2015). Interestingly, our results show that adult quiescent cells acquire the fate of CK8 luminal ductal or mesenchymal cells, without displaying stemness potential *in vitro*. These observations are in line with the study of Kwak and Ghazizadeh (2015) (Kwak and Ghazizadeh, 2015), since they specifically identified label-retaining cells as SMA^+ myoepithelial cells, and $CK19^+$ cells in the striated ducts and the luminal layer of the excretory ducts. The discrepancies between the studies may be explained by EdU pulse-chase model dependency on cellular proliferation. The LRCs analyzed by Chibly et al. (2014) may plausibly not represent completely dormant cells, as minimal one cell division is needed to label these cells, potentially resembling our GFP^{med} group.

Previous studies have relied on the 2D colony-forming technique (Kwak and Ghazizadeh, 2015) or sphere culture (Chibly et al., 2014) for determining the proliferative capabilities of LRC populations. These assays are limited in their ability to recapitulate self-renewal and differentiation potential, which are major characteristics of stem cells. To strengthen our findings, we used a 3D organoid system that allows the long-term expansion of stem/progenitor cells at the single cell level and their progeny (Maimets et al., 2016). Our organoid cultures have shown the differentiation potential of SGSCs both *in vitro* and *in vivo* (Nanduri, 2014; Maimets et al., 2016). Moreover, our model is single-cell based which allows studying individual cellular dynamics (Maimets et al., 2016). Albeit the cellular dynamics of organoids are different from those of slow turnover tissues, in this study we used the organoid model to show the regenerative potential of the selected cells. Particularly, organoid cultures promote the conditional proliferation of cells in response to provided signaling factors, driving them out of dormancy (Fujii and Sato, 2021). We expect that this will include cells which are not cycling *in situ* but do have self-renewal potential when exposed to these factors under our cultured conditions. Moreover, we have shown in several previous (irradiation) studies that organoid forming efficiency can determinate the number of (surviving) putative stem/progenitor cells (Peter et al., 2015; Nagle et al., 2016, 2018). Therefore, the organoid model can reliably be employed to probe the regenerative dynamics of slow tissue LRCs. By using this SMG organoid model, we show that indeed, cells displaying this surrogate measurement of regeneration potential reside in the non-LRC population of the SMG.

Our observations imply that the homeostatic SMG maintenance during postnatal development is sustained by cycling cells. Considering that the SG has a turnover time of 50–125 days (Zajicek et al., 1989; Vissink et al., 2010; Aure et al., 2015), we expected that the replacement of the acinar compartment will mostly occur during the 100 days of chase after embryonic or adult pulse. Although we did not find obvious LRC in the acinar cell compartment, a co-staining with an acinar marker would be needed to solidify this finding. Moreover, within the SG turnover, it appears that only one or two divisions are needed for the generation of a stem/progenitor cell, potentially through plasticity. Cellular plasticity in the SG has been reported as a mechanism orchestrating tissue regeneration after severe damage (Weng et al., 2018; Ninche et al., 2020). Myoepithelial cells, and CK5, Axin 2, CK14, and c-Kit ductal cells have shown dedifferentiation potential to repopulate lost acinar cell populations (Weng et al., 2018; Ninche et al., 2020). Moreover, acinar cells shift to a multipotent state to generate duct cells after ligation injury (Shubin et al., 2020). Our organoid system may simulate this plasticity *in vitro*. $EpCAM^+$ or $CD24^+/CD29^+$ single-sorted cells proliferate and are able to form organoids containing different SG cell types (Nanduri, 2014; Maimets et al., 2016), potentially involving plasticity. As reviewed by Rocchi and colleagues (Rocchi et al., 2021), the exposure of fate-restricted cells to appropriate signaling factors seems to be responsible for the occurrence of plasticity *in vitro*. Therefore, our organoid model shows the lack of stem/progenitor cell and/or plasticity potential of the LRCs per se in the adult SMG.

Interestingly, in contrast to our findings, the contribution of quiescent cells in the maintenance of several tissues based on the H2B-GFP system has been reported, e.g. in the adult liver (Cao et al., 2017), skin (Tumbar et al., 2004), thymus (Dumont-Lagacé et al., 2014), and mammary epithelium (dos Santos et al., 2013). In the pancreas, a model of conservative tissue homeostatic replacement has been proposed. The stem cell maintenance of the homeostatic pancreas is predominantly supported by the self-renewal of mature

pancreatic cells and multipotent progenitors, while dedifferentiation and transdifferentiation rarely occur as reviewed by Lodestijn and colleagues (Lodestijn et al., 2021). Although we cannot exclude that possibility for the SMG, we suggest that the homeostatic postnatal SMG maintenance might be sustained by fate-restricted cycling cells and by the occurrence of plasticity. This is more in line with the case of the mammary gland and the liver. In the adult mammary gland, the homeostatic maintenance is driven by lineage-restricted unipotent stem cells, which give rise to the separate lineages. Additionally, long-lived quiescent mammary gland stem cells can switch to a multipotent proliferative state in response to microenvironmental cues, such as the input of steroid hormones as reviewed by Lee et al. (2019). During homeostasis, the maintenance of the liver has been attributed to the proliferation of mature hepatocytes and cholangiocytes, which self-renew and constitute a supply of mature hepatocytes as reviewed by Miyajima and colleagues (Miyajima et al., 2014). In accordance, we could consider that the SMG, the mammary gland, and the liver are tissues that are homeostatically maintained by the proliferation of lineage-restricted cells and by the occurrence of plasticity. However, in the mammary gland and the liver, both lineage-restricted self-renewal and plasticity are orchestrated by different cellular populations, while in the SMG it seems that the fate-restricted cells may show both unipotency and multipotency. It would be interesting to explore if our findings in the SMG are also occurring in the other SGs, such as the SLG.

Ultimately, our H2B-GFP pulse-chase experiments do suggest the presence of an actively cycling stem/progenitor population within the SG. We report that quiescent cells from embryonic or postnatal origin do not express known putative SG stem/progenitor markers and do not exhibit characteristics of stem/progenitor cells *in vitro*. In the future, it would be important to determine the specific signaling cues required to promote cellular plasticity *in vitro* and *in vivo* of specific SG-differentiated cellular populations.

Limitations of the study

Although our study provides strong evidence of the contribution of non-quiescent cells in the murine SMG developmental dynamics, it is limited to mice due to the *in vivo* lineage-tracing analysis. Moreover, labels only reflect a phenotype but do not necessarily reflect functionality. As reviewed by Rocchi and colleagues (Rocchi et al., 2021), identified murine SG markers have shown a lack of expression or lower potency in human tissue. In addition, the determination of CK5 as a stem/progenitor SG cellular marker has been based on murine embryonic data only (Knox et al., 2010; Lombaert et al., 2013). Therefore, it should be considered the use of functional assays to further confirm our findings in humans.

STAR★METHODS

Detailed methods are provided in the online version of this paper and include the following:

- KEY RESOURCES TABLE
- RESOURCE AVAILABILITY
  - Lead contact
  - Materials availability
  - Data and code availability
- EXPERIMENTAL MODEL AND SUBJECT DETAILS
  - Mice
- METHOD DETAILS
  - Two-photon microscopy
  - Whole-organ confocal microscopy
  - Immunostaining
  - Cell sorting and single cell SG organoid culture
  - Self-renewal assay
- QUANTIFICATION AND STATISTICAL ANALYSIS

SUPPLEMENTAL INFORMATION

Supplemental information can be found online at https://doi.org/10.1016/j.isci.2022.105047.

ACKNOWLEDGMENTS

This work was supported by grants from The Netherlands Organization for Health Research and Development (ZonMW-Grant nr. 11.600.1023), the Netherlands Institute for Regenerative Medicine (NIRM, Grant

No. FE0908), the Dutch Cancer Society (RUG2013-5792 and grant number 12092), and the Graduate School of Medical Sciences, University of Groningen, The Netherlands (PhD grant awarded to Paola Serrano Martinez). Part of the work has been performed at the UMCG Microscopy and Imaging Center (UMIC), which is sponsored by an NWO grant (175-010-2009-023). Martti Maimets was supported by SA Archimedes DoRa program. We thank K. Sjollema for expert assistance in confocal microscopy and G. Mesander and H. Moes for expert cell sorting assistance. The Graphical abstract was designed using the BioRender web tool.

AUTHOR CONTRIBUTIONS

P.S.M.: Data curation; Formal analysis; Funding acquisition; Investigation; Methodology; Visualization; Writing-original draft. M.M.: Conceptualization; Data curation; Formal analysis; Funding acquisition; Investigation; Methodology; Visualization; Writing- original draft. R.B.: Investigation; Methodology. R.v.O., G.d.H., S.P.: Conceptualization; Supervision; Writing-review & editing. R.P.C.: Conceptualization; Funding acquisition; Supervision; Visualization; Writing-review & editing.

DECLARATION OF INTERESTS

The authors declare no competing interests.

Received: February 4, 2022
Revised: June 8, 2022
Accepted: August 26, 2022
Published: October 21, 2022

REFERENCES

Aure, M.H., Konieczny, S.F., and Ovitt, C.E. (2015). Salivary gland homeostasis is maintained through acinar cell self-duplication. Dev. Cell *33*, 231–237. https://doi.org/10.1016/j.devcel.2015.02.013.

Barker, N., van Es, J.H., Kuipers, J., Kujala, P., van den Born, M., Cozijnsen, M., Haegebarth, A., Korving, J., Begthel, H., Peters, P.J., and Clevers, H. (2007). Identification of stem cells in small intestine and colon by marker gene Lgr5. Nature *449*, 1003–1007. https://doi.org/10.1038/nature06196.

Cao, W., Chen, K., Bolkestein, M., Yin, Y., Verstegen, M.M.A., Bijvelds, M.J.C., Wang, W., Tuysuz, N., Ten Berge, D., Sprengers, D., et al. (2017). Dynamics of proliferative and quiescent stem cells in liver homeostasis and injury. Gastroenterology *153*, 1133–1147. https://doi.org/10.1053/j.gastro.2017.07.006.

Chacón-Martínez, C.A., Koester, J., and Wickström, S.A. (2018). Signaling in the stem cell niche: regulating cell fate, function and plasticity. Development *145*, dev165399. https://doi.org/10.1242/dev.165399.

Cheung, T.H., and Rando, T.A. (2013). Molecular regulation of stem cell quiescence. Nat. Rev. Mol. Cell Biol. *14*, 329–340. https://doi.org/10.1038/nrm3591.

Chibly, A.M., Querin, L., Harris, Z., and Limesand, K.H. (2014). Label-retaining cells in the adult murine salivary glands possess characteristics of adult progenitor cells. PLoS One *9*, e107893. https://doi.org/10.1371/journal.pone.0107893.

Clayton, E., Doupé, D.P., Klein, A.M., Winton, D.J., Simons, B.D., and Jones, P.H. (2007). A single type of progenitor cell maintains normal epidermis. Nature *446*, 185–189. https://doi.org/10.1038/nature05574.

Collins, C.A., Olsen, I., Zammit, P.S., Heslop, L., Petrie, A., Partridge, T.A., and Morgan, J.E. (2005). Stem cell function, self-renewal, and behavioral heterogeneity of cells from the adult muscle satellite cell niche. Cell *122*, 289–301. https://doi.org/10.1016/j.cell.2005.05.010.

Cotroneo, E., Proctor, G.B., Paterson, K.L., and Carpenter, G.H. (2008). Early markers of regeneration following ductal ligation in rat submandibular gland. Cell Tissue Res. *332*, 227–235. https://doi.org/10.1007/s00441-008-0588-6.

Cotroneo, E., Proctor, G.B., and Carpenter, G.H. (2010). Regeneration of acinar cells following ligation of rat submandibular gland retraces the embryonic-perinatal pathway of cytodifferentiation. Differentiation. *79* (2), 120–130. https://doi.org/10.1016/j.diff.2009.11.005.

dos Santos, C.O., Rebbeck, C., Rozhkova, E., Valentine, A., Samuels, A., Kadiri, L.R., Osten, P., Harris, E.Y., Uren, P.J., Smith, A.D., and Hannon, G.J. (2013). Molecular hierarchy of mammary differentiation yields refined markers of mammary stem cells. Proc. Natl. Acad. Sci. USA *110*, 7123–7130. https://doi.org/10.1073/pnas.1303919110.

Dumont-Lagacé, M., Brochu, S., St-Pierre, C., and Perreault, C. (2014). Adult thymic epithelium contains nonsenescent label-retaining cells. J. Immunol. *192*, 2219–2226. https://doi.org/10.4049/jimmunol.1302961.

Emmerson, E., May, A.J., Berthoin, L., Cruz-Pacheco, N., Nathan, S., Mattingly, A.J., Chang, J.L., Ryan, W.R., Tward, A.D., and Knox, S.M. (2018). Salivary glands regenerate after radiation injury through SOX2-mediated secretory cell replacement. EMBO Mol. Med. *10*, e8051. John Wiley & Sons, Ltd. https://doi.org/10.15252/emmm.201708051.

Eriksson, J.E., Dechat, T., Grin, B., Helfand, B., Mendez, M., Pallari, H.M., and Goldman, R.D. (2009). Introducing intermediate filaments: from discovery to disease. J. Clin. Invest. *119*, 1763–1771. https://doi.org/10.1172/JCI38339.

Foudi, A., Hochedlinger, K., Van Buren, D., Schindler, J.W., Jaenisch, R., Carey, V., and Hock, H. (2009). Analysis of histone 2B-GFP retention reveals slowly cycling hematopoietic stem cells. Nat. Biotechnol. *27*, 84–90. https://doi.org/10.1038/nbt.1517.

Fuchs, E. (2009). The tortoise and the hair: slow-cycling cells in the stem cell race. Cell *137*, 811–819. https://doi.org/10.1016/j.cell.2009.05.002.

Fujii, M., and Sato, T. (2021). Somatic cell-derived organoids as prototypes of human epithelial tissues and diseases. Nat. Mater. *20*, 156–169. https://doi.org/10.1038/s41563-020-0754-0.

Hisatomi, Y., Okumura, K., Nakamura, K., Matsumoto, S., Satoh, A., Nagano, K., Yamamoto, T., and Endo, F. (2004). Flow cytometric isolation of endodermal progenitors from mouse salivary gland differentiate into hepatic and pancreatic lineages. Hepatology *39*, 667–675. https://doi.org/10.1002/hep.20063.

Hsu, Y.-C., and Fuchs, E. (2012). A family business: stem cell progeny join the niche to regulate homeostasis. Nat. Rev. Mol. Cell Biol. *13*, 103–114. https://doi.org/10.1038/nrm3272.

Jadhav, U., Saxena, M., O'Neill, N.K., Saadatpour, A., Yuan, G.C., Herbert, Z., Murata, K., and Shivdasani, R.A. (2017). Dynamic reorganization of chromatin accessibility signatures during dedifferentiation of secretory precursors into Lgr5+ intestinal stem cells. Cell Stem Cell *21*, 65–77. Elsevier. https://doi.org/10.1016/j.stem.2017.05.001.

Kim, Y.-J., Kwon, H.J., Shinozaki, N., Hashimoto, S., Shimono, M., Cho, S.W., and Jung, H.S. (2008). Comparative analysis of ABCG2-expressing and label-retaining cells in mouse submandibular gland. Cell Tissue Res. *334*, 47–53. https://doi.org/10.1007/s00441-008-0667-8.

Kimoto, M., Yura, Y., Kishino, M., Toyosawa, S., and Ogawa, Y. (2008). Label-retaining cells in the rat submandibular gland. J. Histochem. Cytochem. *561*, 15–24. https://doi.org/10.1369/jhc.7A7269.2007.

Knox, S.M., Lombaert, I.M.A., Reed, X., Vitale-Cross, L., Gutkind, J.S., and Hoffman, M.P. (2010). Parasympathetic innervation maintains epithelial progenitor cells during salivary organogenesis. Science *329*, 1645–1647. https://doi.org/10.1126/science.1192046.

Knox, S.M., Lombaert, I.M.A., Haddox, C.L., Abrams, S.R., Cotrim, A., Wilson, A.J., and Hoffman, M.P. (2013). Parasympathetic stimulation improves epithelial organ regeneration. Nat. Commun. *4*, 1494. https://doi.org/10.1038/ncomms2493.

Kwak, M., and Ghazizadeh, S. (2015). Analysis of histone H2BGFP retention in mouse submandibular gland reveals actively dividing stem cell populations. Stem Cell. Dev. *24*, 565–574. Mary Ann Liebert, Inc.. https://doi.org/10.1089/scd.2014.0355

Kwak, M., Alston, N., and Ghazizadeh, S. (2016). Identification of stem cells in the secretory complex of salivary glands. J. Dent. Res. *95*, 776–783. SAGE Publications. https://doi.org/10.1177/0022034516634664.

Lee, E., Piranlioglu, R., Wicha, M.S., and Korkaya, H. (2019). Plasticity and potency of mammary stem cell subsets during mammary gland development. Int. J. Mol. Sci. *20*, 2357. https://doi.org/10.3390/ijms20092357.

Lodestijn, S.C., van Neerven, S.M., Vermeulen, L., and Bijlsma, M.F. (2021). Stem cells in the exocrine pancreas during homeostasis, injury, and cancer. Cancers *13*, 3295. https://doi.org/10.3390/cancers13133295.

Lombaert, I.M.A., Brunsting, J.F., Wierenga, P.K., Faber, H., Stokman, M.A., Kok, T., Visser, W.H., Kampinga, H.H., de Haan, G., and Coppes, R.P. (2008). Rescue of salivary gland function after stem cell transplantation in irradiated glands. PLoS One *3*, e2063. https://doi.org/10.1371/journal.pone.0002063.

Lombaert, I.M., Abrams, S.R., Li, L., Eswarakumar, V.P., Sethi, A.J., Witt, R.L., and Hoffman, M.P. (2013). Combined KIT and FGFR2b signaling regulates epithelial progenitor expansion during organogenesis. Stem Cell Rep. *1*, 604–619. Elsevier. https://doi.org/10.1016/j.stemcr.2013.10.013.

MacDONALD, R.A. (1961). Lifespan" of liver cells: autoradiographic study using tritiated thymidine in normal, cirrhotic, and partially hepatectomized rats. Arch. Intern. Med. *107*, 335–343. https://doi.org/10.1001/archinte.1961.03620030023003.

Magami, Y., Azuma, T., Inokuchi, H., Kokuno, S., Moriyasu, F., Kawai, K., and Hattori, T. (2002). Cell proliferation and renewal of normal hepatocytes and bile duct cells in adult mouse liver. Liver *22*, 419–425. https://doi.org/10.1034/j.1600-0676.2002.01702.x.

Maimets, M., Rocchi, C., Bron, R., Pringle, S., Kuipers, J., Giepmans, B.N.G., Vries, R.G.J., Clevers, H., de Haan, G., van Os, R., and Coppes, R.P. (2016). 'Long-Term in vitro expansion of salivary gland stem cells driven by Wnt signals. Stem Cell Rep. *6*, 150–162. https://doi.org/10.1016/j.stemcr.2015.11.009.

Miyajima, A., Tanaka, M., and Itoh, T. (2014). Stem/progenitor cells in liver development, homeostasis, regeneration, and reprogramming. Cell Stem Cell *14*, 561–574. https://doi.org/10.1016/j.stem.2014.04.010.

Miyaoka, Y., Ebato, K., Kato, H., Arakawa, S., Shimizu, S., and Miyajima, A. (2012). Hypertrophy and unconventional cell division of hepatocytes underlie liver regeneration. Curr. Biol. *22*, 1166–1175. https://doi.org/10.1016/j.cub.2012.05.016.

Nagle, P.W., Hosper, N.A., Ploeg, E.M., van Goethem, M.J., Brandenburg, S., Langendijk, J.A., Chiu, R.K., and Coppes, R.P. (2016). The in vitro response of tissue stem cells to irradiation with different linear energy transfers. Int. J. Radiat. Oncol. Biol. Phys. *95*, 103–111. https://doi.org/10.1016/j.ijrobp.2016.02.020.

Nagle, P.W., Hosper, N.A., Barazzuol, L., Jellema, A.L., Baanstra, M., van Goethem, M.J., Brandenburg, S., Giesen, U., Langendijk, J.A., van Luijk, P., and Coppes, R.P. (2018). Lack of DNA damage response at low radiation doses in adult stem cells contributes to organ dysfunction. Clin. Cancer Res. *24*, 6583–6593. https://doi.org/10.1158/1078-0432.CCR-18-0533.

Nanduri, L.S.Y., Maimets, M., Pringle, S.A., van der Zwaag, M., van Os, R.P., and Coppes, R.P. (2011). Regeneration of irradiated salivary glands with stem cell marker expressing cells. Radiother. Oncol. *99*, 367–372. https://doi.org/10.1016/j.radonc.2011.05.085.

Nanduri, L.S., Baanstra, M., Faber, H., Rocchi, C., Zwart, E., De Haan, G., Van Os, R., and Coppes, R.P. (2014). Purification and Ex Vivo expansion of fully functional salivary gland stem cells. Stem Cell Rep. *3*, 957–964. Elsevier. https://doi.org/10.1016/j.stemcr.2014.09.015.

Ninche, N., Kwak, M., and Ghazizadeh, S. (2020). Diverse epithelial cell populations contribute to the regeneration of secretory units in injured salivary glands. Development *147*, dev192807. https://doi.org/10.1242/dev.192807.

Osailan, S.M., Proctor, G.B., McGurk, M., and Paterson, K.L. (2006). Intraoral duct ligation without inclusion of the parasympathetic nerve supply induces rat submandibular gland atrophy. Int. J. Exp. Pathol. *87*, 41–48. Blackwell Science Inc. https://doi.org/10.1111/j.0959-9673.2006.00453.x.

Pepe-Mooney, B.J., Dill, M.T., Alemany, A., Ordovas-Montanes, J., Matsushita, Y., Rao, A., Sen, A., Miyazaki, M., Anakk, S., Dawson, P.A., et al. (2019). Single-cell analysis of the liver epithelium reveals dynamic heterogeneity and an essential role for YAP in homeostasis and regeneration. Cell Stem Cell *25*, 23–38. Elsevier. https://doi.org/10.1016/j.stem.2019.04.004.

Peter, van L., Pringle, S., Deasy, J.O., Moiseenko, V.V., Faber, H., Hovan, A., Baanstra, M., van der Laan, H.P., Kierkels, R.G., van der Schaaf, A., et al. (2015). Sparing the region of the salivary gland containing stem cells preserves saliva production after radiotherapy for head and neck cancer. Sci. Transl. Med. *7*, 305ra147. American Association for the Advancement of Science. https://doi.org/10.1126/scitranslmed.aac4441.

Post, Y., and Clevers, H. (2019). Defining adult stem cell function at its simplest: the ability to replace lost cells through mitosis. Cell Stem Cell *25*, 174–183. https://doi.org/10.1016/j.stem.2019.07.002.

Pringle, S., Maimets, M., van der Zwaag, M., Stokman, M.A., van Gosliga, D., Zwart, E., Witjes, M.J.H., de Haan, G., van Os, R., and Coppes, R.P. (2016). Human salivary gland stem cells functionally restore radiation damaged salivary glands. Stem Cell. *34*, 640–652. https://doi.org/10.1002/stem.2278.

Rocchi, C., Barazzuol, L., and Coppes, R.P. (2021). The evolving definition of salivary gland stem cells. NPJ Regen. Med. *6*, 4. Nature Publishing Group UK. https://doi.org/10.1038/s41536-020-00115-x.

Shubin, A.D., Sharipol, A., Felong, T.J., Weng, P.L., Schutrum, B.E., Joe, D.S., Aure, M.H., Benoit, D.S.W., and Ovitt, C.E. (2020). Stress or injury induces cellular plasticity in salivary gland acinar cells. Cell Tissue Res. *380*, 487–497. https://doi.org/10.1007/s00441-019-03157-w.

Takahashi, S., Shinzato, K., Domon, T., et al. (2004a). Mitotic proliferation of myoepithelial cells during regeneration of atrophied rat submandibular glands after duct ligation. J. Oral Pathol. Med. *33*, 430–434. John Wiley & Sons, Ltd. https://doi.org/10.1111/j.1600-0714.2004.00234.x.

Takahashi, S., Shinzato, K., Nakamura, S., et al. (2004b). Cell death and cell proliferation in the regeneration of atrophied rat submandibular glands after duct ligation. J. Oral Pathol. Med. *33*, 23–29. John Wiley & Sons, Ltd. https://doi.org/10.1111/j.1600-0714.2004.00191.x.

Tetteh, P.W., Basak, O., Farin, H.F., Wiebrands, K., Kretzschmar, K., Begthel, H., van den Born, M., Korving, J., De Sauvage, F., Van Es, J.H., et al. (2016). Replacement of lost Lgr5-Positive stem cells through plasticity of their enterocyte-lineage daughters. Cell Stem Cell *18*, 203–213. Elsevier. https://doi.org/10.1016/j.stem.2016.01.001.

Tumbar, T., Guasch, G., Greco, V., Blanpain, C., Lowry, W.E., Rendl, M., and Fuchs, E. (2004). Defining the epithelial stem cell niche in skin. Science *303*, 359–363. https://doi.org/10.1126/science.1092436.

van Velthoven, C.T.J., and Rando, T.A. (2019). Stem cell quiescence: dynamism, restraint, and cellular idling. Cell Stem Cell *24*, 213–225. Elsevier. https://doi.org/10.1016/j.stem.2019.01.001.

Vissink, A., Mitchell, J.B., Baum, B.J., Limesand, K.H., Jensen, S.B., Fox, P.C., Elting, L.S., Langendijk, J.A., Coppes, R.P., and Reyland, M.E. (2010). Clinical management of salivary gland hypofunction and xerostomia in head-and-neck cancer patients: successes and barriers. Int. J. Radiat. Oncol. Biol. Phys. *78*, 983–991. https://doi.org/10.1016/j.ijrobp.2010.06.052.

Weng, P.-L., Aure, M.H., Maruyama, T., and Ovitt, C.E. (2018). Limited regeneration of adul salivary

glands after severe injury involves cellular plasticity. Cell Rep. *24*, 1464–1470.e3. https://doi.org/10.1016/j.celrep.2018.07.016.

Wilson, A., Laurenti, E., Oser, G., van der Wath, R.C., Blanco-Bose, W., Jaworski, M., Offner, S., Dunant, C.F., Eshkind, L., Bockamp, E., et al. (2008). Hematopoietic stem cells reversibly switch from dormancy to self-renewal during homeostasis and repair. Cell *135*, 1118–1129. https://doi.org/10.1016/j.cell.2008.10.048.

Xiao, N., Lin, Y., Cao, H., Sirjani, D., Giaccia, A.J., Koong, A.C., Kong, C.S., Diehn, M., and Le, Q.T. (2014). Neurotrophic factor GDNF promotes survival of salivary stem cells. J. Clin. Invest. *124*, 3364–3377. https://doi.org/10.1172/JCI74096.

Yang, B., Treweek, J.B., Kulkarni, R.P., Deverman, B.E., Chen, C.K., Lubeck, E., Shah, S., Cai, L., and Gradinaru, V. (2014). Single-cell phenotyping within transparent intact tissue through whole-body clearing. Cell *158*, 945–958. https://doi.org/10.1016/j.cell.2014.07.017.

Zajicek, G., Schwartz-Arad, D., Arber, N., and Michaeli, Y. (1989). The streaming of the submandibular gland II: parenchyma and stroma advance at the same velocity. Cell Prolif. *22*, 343–348. John Wiley & Sons, Ltd. https://doi.org/10.1111/j.1365-2184.1989.tb00219.x.

STAR★METHODS

KEY RESOURCES TABLE

REAGENT or RESOURCE	SOURCE	IDENTIFIER
Antibodies		
Anti-Green Fluorescent Protein Antibody	Merck-Millipore	MAB3580
Anti-Cytokeratin 14 Antibody	Abcam	ab175549
Anti-Keratin 5 Antibody	Covance	PRB-160-P
Krt8 Antibody	Developmental Studies Hybridoma Bank	TROMA-I
Vimentin (C-20)	Santa Cruz Biotechnology	sc-7557
Goat anti-Mouse IgG (H + L) Secondary Antibody, Alexa Fluor® 488 conjugate	Thermo Fisher Scientific	A-11001
Goat anti-Rabbit IgG (H + L) Secondary Antibody, Alexa Fluor® 594 conjugate	Thermo Fisher Scientific	A-11012
Donkey anti-Goat IgG (H + L) Secondary Antibody, Alexa Fluor® 594 conjugate	Thermo Fisher Scientific	A-11058
Anti-Mouse CD31 (PECAM-1) PE	eBioscience	12–0311
PE anti-mouse CD45	BioLegend	103106
PE/Cy7 anti-mouse TER-119/Erythroid Cells	BioLegend	116222
APC anti-mouse/rat CD29 Antibody	BioLegend	Cat# 102216; RRID: AB_492833
Pacific Blue™ anti-mouse CD24 Antibody	BioLegend	Cat# 101820; RRID: AB_572011
Anti-Cytokeratin 14 Antibody,	Abcam	Cat#: ab175549; RRID: AB_2923353
Chemicals, peptides, and recombinant proteins		
Doxycycline hyclate	Sigma	D9891
VA-044	FUJIFILM Wako Pure Chemical Corporation	CAS RN® 27776-21-2
eBioscience™ DRAQ5™	Invitrogen	65-0880
Histodenz™	Sigma	D2158
Sodium azide	Merck	822335
Matrigel	Vwr	356235
0.05% Tryosin-EDTA	Invitrogen (Gibco Life Technologies)	25300–096
Propidium iodide	Sigma	P4170
Magnesium sulfate	Sigma-Aldrich	M7506
DNase I	Roche	11284932001
Dispase	Gibco/Invitrogen	17105–041
Collagenase type II	Gibco/Invitrogen	17101–015
Hyaluronidase	Sigma	H3506-5G
$CaCl_2$	Sigma	C3306 SIGMA
N2 Supplement	Gibco	17502–048
EGF	Sigma	E9644
FGF2	Preprotech- Bioconnect	100–18B
Dexamethasone	Sigma	d4902-25mg
Insulin	Sigma	I6634-100MG

(*Continued on next page*)

Continued

REAGENT or RESOURCE	SOURCE	IDENTIFIER
Y-27632 dihydrochloride Rho-Kinase inhibitor	Bioconnect-Abcam	ab120129
Glutamax	Thermo Fisher Scientific	35050038
Pen/Strep	Invitrogen	15140–163
DMEM F12 (Dulbecco's modified Eagle's medium: F12)	Gibco/Invitrogen	11320–074
Wnt3a conditioned media	Clevers's lab gift	N/A
R-spondin1 conditioned media	Clevers's lab gift	N/A
DAB (3.3′-diaminobenzide)	Sigma	D4168-50set
DAPI	Thermo Fisher Scientific/Pierce	62247
Tween-20	Sigma	P1379-500ML
Formaldehyde solution	Sigma	252549-1L
Hematoxylin	Sigma	H3136-25G
Critical commercial assays		
Vectastatin® ABC kit	Vector	PK-6100
Experimental models: Organisms/strains		
B6;129S4-*Gt(ROSA)26Sortm1(rtTA*M2) JaeCol1a1tm7(tetO-HIST1H2BJ/GFP)Jae*/J	The Jackson Laboratory	016836
Software and algorithms		
Imaris for Cell Biologists	Oxford Instruments	https://imaris.oxinst.com/products/imaris-for-cell-biologists?gclid=Cj0KCQiA9OiPBhCOARIsAI0y71D6f7nA5PWuRcp_rsPrx4axRbngkq8QT89eTO8rtfVE_vv7_FOQSIoaApfHEALw_wcB
ZEISS ZEN lite	ZEISS	https://www.zeiss.com/microscopy/int/products/microscope-software/zen-lite.html
Prism 9	GraphPad	https://www.graphpad.com/scientific-software/prism/

RESOURCE AVAILABILITY

Lead contact

Further information and requests for resources should be directed to and will be fulfilled by the lead contact, Rob P Coppes (r.p.coppes@umcg.nl).

Materials availability

This study did not generate new unique reagents.

Data and code availability

- All data reported in this paper will be shared by the lead contact upon request.
- This paper does not report original code.
- Any additional information required to reanalyze the data reported in this paper is available from the lead contact upon request.

EXPERIMENTAL MODEL AND SUBJECT DETAILS

Mice

B6;129S4-*Gt(ROSA)26Sortm1(rtTA*M2)JaeCol1a1tm7(tetO-HIST1H2BJ/GFP)Jae*/J were purchased from the Jackson Laboratory. Animals were bred as homozygotes in the Central Animal Facility of University Medical Centre Groningen. The mice were maintained under conventional conditions and fed *ad libitum* with food pellets (RMH-B, Hope Farms B.V.) and water. Both males and females were used for transgene expression. Doxycycline (Sigma D9891, 2 mg/mL, supplemented with sucrose at 10 mg/mL) was administered to the pregnant female mother in drinking water or with doxycycline-impregnated food pellets (SDS

Tecnilab, 625 ppm RM1) during embryonic development. To induce transgene expression during adulthood, doxycycline-impregnated food pellets (SDS Tecnilab, 625 ppm RM1) were used. All experiments were approved by the Ethical Committee on animal testing of the University of Groningen.

METHOD DETAILS

Two-photon microscopy

Postnatal H2B-GFP (P1) SGs were harvested and the epithelium and fat were separated by dispase (Gibco, 1 mg/mL) treatment for 15 min at 37°C. Cleaned SGs were mounted in PBS and processed for imaging. Imaging was performed by using Zeiss 7 MP multiphoton system (Zeiss). For two-photon microscopy of green (GFP) fluorophore, the laser (Coherent) was tuned to ~970 nm (940–970 nm). A 20× dipping objective (Zeiss W Plan A 20×, 1.0 NA) was used for these experiments. 3D reconstruction was performed using Imaris (Bitplane) software.

Whole-organ confocal microscopy

Adult H2B-GFP pulsed and chased (P40 and P60) mouse SGs were harvested, bisected longitudinally and processed for tissue clearing as reported by Yang and colleagues (Yang et al., 2014). SGs were fixed in 4% formaldehyde solution overnight. Subsequently, fixed tissue sections were incubated at 4°C overnight in AP40 solution (4% acrylamide in PBS) supplemented with 0.25% photo initiator VA-044 (Wako Chemicals), degassed with nitrogen for 1–5 min and then incubated for 2–3 h at 37°C to initiate tissue-hydrogel hybridization after which tissue-hydrogel matrices were transferred to 8% SDS in 0.1 M PBS (pH7.5) and incubated for 5 days. Prior to counterstaining with DRAQ5™ (eBioscience) matrices were washed with PBS over the course of 1 day followed by mounting in RIMS imaging media containing 40 g of Histodenz™ (Sigma) in 30 mL of 0.02 M PB with 0.1% tween-20 and 0.01% sodium azide (pH 7.5). Confocal microscopy was carried out on a LSM780 system (Zeiss) using Zen software. PlnApo 20×, 0.8 NA DICII lens was used with 488 and 633 laser lines. Image stitching was performed using Zen (Zeiss) software and 3D reconstruction was achieved using Imaris (Bitplane) software.

Immunostaining

SGs from H2B-GFP pulsed and chased mice were 4% formaldehyde fixed (24 hours, RT) and processed for paraffin embedding. Following dehydration, the tissue was embedded in paraffin and sliced into 4 μm sections. For immunofluorescence staining, the sections were dewaxed, boiled for 8 min in pre-heated 10 mM citric acid retrieval buffer (pH 6.0) containing 0.05% Tween-20, washed thoroughly prior to primary antibody exposure and labeled for the following markers: GFP (1:100, Chemicon, MAB3580), CK14 (1:400, Abcam, ab175549), CK5 (1:100, Covance, PRB-160-P), CK8 (1:50, Hybridoma bank, TROMA-I) Vimentin (1:50, Santa Cruz, sc-7557). For fluorescence microscopy Goat anti-Mouse Alexa Fluor 488 (Thermo Fisher Scientific, A-11001), Goat anti-Rabbit Alexa Fluor® 594 (Thermo Fisher Scientific, A-11012) or Donkey anti-Goat IgG Alexa Fluor® 594 (Thermo Fisher Scientific, A-11058) conjugates at 1:300 dilution were used as secondary antibodies. Nuclear staining was performed with DAPI (Sigma-Aldrich). Visualization for bright-field microscopy was accomplished by addition of specific secondary biotin-carrying antibodies (Dako). A VECTASTAIN® ABC kit (Vector labs) was used followed by 3.3′-diaminobenzide (DAB) kit to detect positive staining. Nuclear staining was performed with hematoxylin. Images were acquired with Leica DM6000 B microscope using LAS AF software or Leica DM6 B microscope using LAS X software.

Cell sorting and single cell SG organoid culture

SGs were harvested from adult pulsed and chased H2B-GFP mice, mechanically disrupted by gentleMACS Dissociator (Milteny) followed by enzymatic digestion with collagenase type II (0,63 mg/mL; Gibco), hyaluronidase (0,5 mg/mL; Sigma-Aldrich) and $CaCl_2$ (6,25 mM; Sigma-Aldrich). After filtering through 100 μm cell strainer the suspension was dissociated using 0,05% trypsin-EDTA (Gibco) following filtering through 35 μm strainer. Cell pellets were incubated with anti-mouse CD31 PE (eBioscience, 12-0311-82), PE anti-mouse CD45 (Biolegend, 103106) and PE/Cy7 anti-mouse TER-119/Erythroid Cells (Biolegend, 116222) antibodies for 15′ at room temperature. After washing thoroughly cells were suspended in a solution containing propidium iodide (PI, 1 mg/mL, Sigma-Aldrich, P4170), Magnesium sulfate (10 mM, Sigma-Aldrich, M7506) and DNase I (50 μg/mL, Roche, 11284932001). Pulse-width gating excluded cell doublets while dead cells were excluded by gating on PI negative cells. Positive gating was based on the comparison of non-stained and single antibody-stained samples in the case of CD31, CD45 and Ter-119 and on the comparison of not-induced and induced H2B-GFP mice in the case of GFP. Sorted cells were embedded

in Matrigel (Vwr) and seeded in 12-well plates. Cells were cultured in WRY medium (DMEM/F12 containing Pen/Strep antibiotics [1×, Invitrogen], Glutamax [1×, Invitrogen], N2 [1×, Gibco], EGF [20 ng/mL, Sigma-Aldrich], FGF2 [20 ng/mL, Sigma-Aldrich], insulin [10 μg/mL, Sigma-Aldrich], dexamethasone [1 μM, Sigma-Aldrich], Y-27632 [10 μM, Sigma-Aldrich], 10% R-spondin1 conditioned medium and 50% Wnt3a conditioned medium).

Self-renewal assay

Twelve-day organoid cultures were dispersed to single cell suspension using 0.05% trypsin-EDTA (Gibco). 25 μL of suspension containing 10 000 cells was combined with 50 μL of Matrigel and deposited in the center of 12-well tissue culture plates and covered in WRY medium. 7 days after seeding Matrigel was dissolved by incubation with dispase (1 mg/mL; Gibco) for 30 min at 37ºC. Organoids released from the gels were again processed to a single cell suspension, cell number and organoid number noted, and encapsulation in Matrigel repeated. This cycle was repeated up to 3 times (3 passages).

QUANTIFICATION AND STATISTICAL ANALYSIS

All values are represented as mean ± standard error of the mean (SEM) (**$p < 0.01$). Student's t-test was used for testing statistical significance in cell sorting and cell culture experiments. Numbers for tested groups throughout experiments equal at least 3. All calculations were performed using GraphPad Prism (GraphPad software) software.